Controlling a Non-Linear Space Robot using Linear Controllers

A. W. I. Mohamed, C. M. Saaj, A. Seddaoui and S. Eckersley

Abstract Space robots have been under intensive consideration to perform various in-orbit operations like the servicing of satellites, assembly of large structures, maintenance of other space assets and debris removal. Such orbital missions require a servicer spacecraft equipped with one or more dexterous manipulators. However, unlike its terrestrial counterparts, the base of the robotic manipulator is not fixed in inertial space. Additionally, the system will be subjected to extreme space environmental perturbations, parametric uncertainties as well as system constraints due to the dynamic coupling between the manipulator and the base-spacecraft. This paper presents the dynamic model of the space robot and a three-stage control algorithm to control such a highly non-linear system. In this approach, Feed-Forward compensation and Feed-Forward Linearization techniques are used to decouple and linearize the system, therefore allowing the testing of the linear PID and LQR controllers as final stages. Moreover, a simulation-based trade-off analysis was conducted to assess the efficacy of the proposed controllers. This assessment considered the requirements on precise trajectory tracking, minimizing power consumption and robustness during the close-range operation with the target spacecraft.

1 Introduction

Orbital robotic missions have several benefits, from the disposal of orbital debris or dead spacecraft, to extending the life of unique, high-value assets such as the International Space Station (ISS) or the Hubble Space Telescope (HST), to refueling and repairing of commercial satellites as a more economical alternative [1], [2]. Extending the life of such space systems, and hence reducing the associated costs, will require capture, repair, maintenance, and assembly capabilities in orbit. Currently, these servicing tasks are being accomplished manually by astronaut's Extravehicular activity (EVA). However, time restrictions for the maneuver, cost of human life support facilities, and the high risks that astronauts face are some serious restrictions for EVA [3]. Additionally, beyond LEO, high-value satellites occupy valuable orbital slots where any faulty ones represent a threat for other spacecraft in MEO or GEO as the presence of humans is currently not possible in higher Earth orbits [4]. Other benefits of using space robots are the reduction in design, manufacturing and launch costs by approximately $20,000/Kg [5]. Moreover, space robots offer technology refresh, in which certain components such as electronics or mirrors are periodically replaced to cope with the technological advancements.

On the other hand, after 60 years of uncontrolled debris proliferation and intensive space use, Earth orbits have reached a shifting point, known as the "Kessler syndrome", where human intervention is needed [6]. A forecast for the upcoming

A. W. I. Mohamed, C. M. Saaj and A. Seddaoui, Surrey Space Centre, University of Surrey, Guildford GU2 7XH, UK. Emails: AmrWahied.Mohamed@gmail.com, c.saaj@surrey.ac.uk, a.seddaoui@surrey.ac.uk.

Steve Eckersley, Surrey Satellite Technology Ltd, Guildford GU2 7YE, UK, Email: S.Eckersley@sstl.co.uk

200 years' states that access to space would almost be impossible if nothing else is done. Therefore, in order to mitigate debris proliferation, several solutions have been proposed, including: electrodynamic tethers, Earth-based pulsed laser, or even capturing debris using harpoons and nets [6]. Considering the limitations of these approaches, space robots might be a better alternative to capture a wide range of targets in orbit [6]. However, unlike fixed-based manipulators, the base of the space manipulator is no longer fixed in the inertial space, therefore, it introduces a high level of kinematic and dynamic complexity making it challenging to control the space robot. Moreover, due to the mutual dynamic coupling between the base-spacecraft and the manipulator, reaction forces and moments will be generated during the motion of the manipulator. This is in addition to the issues caused by excitation of vibration of the solar paddles on-board. Moreover, the severity of these effects depends on the mass ratios between the manipulator and the base-spacecraft; a threshold of up to one third is when these effects become more dominant. Additionally, the centre of mass of the overall system changes continuously during the motion of the manipulator [3], and the system is subjected to external environmental perturbations like the Gravity Gradient, Aerodynamic Drag, Solar Pressure, Residual Magnetic disturbances as well as parametric uncertainties. Hence, it is challenging to develop a high-performance controller with sufficient robustness to withstand all the aforementioned disturbances.

This paper is organized as follows: Section 2 gives a literature review of the space robot and a detailed explanation of the different approaches of operating a space robot, highlighting the pros and cons of each, Section 3 then establishes the mathematical model of the dynamics and kinematics of Controlled-Floating space robots, Section 4 gives a breakdown of the external perturbations resulting from the space environment, as well as the effects of parametric uncertainties on the system, Section 5 illustrates the control algorithms used for the trajectory tracking of the end-effector of the manipulator, and Section 6 discusses the simulation results and presenting a trade-off analysis between PID and LQR controllers as a final stage of the control algorithm. Finally, it ends with the main conclusions and future work in Section 7.

2 State-of-the-art on Space Robots

2.1 Modes of operation

Traditionally, there are two major approaches for operating a space robot: one links the AOCS of the spacecraft with the manipulator's controller, while the other allows the base-spacecraft to move freely in reaction to the manipulator's motion. They are called Free-Flying and Free-Floating configurations respectively [6]. In the Free-Flying approach, the controller of the base-spacecraft tries to maintain a constant attitude and position. Therefore, the base of the manipulator can be considered as being fixed in inertial space; thus, all the angular characteristics are similar to its Earth-based counterpart. Accordingly, the rotational matrix of the composite 4x4 Denavit-Hartenberg matrix will have the same format as in the terrestrial manipulator. However, the spacecraft bus platform has to employ excessive attitude control using Reaction Wheels (RWs) or thrusters to maintain almost constant position and

attitude during the operation of the manipulator. Such systems have a high level of redundancy and versatility on one hand, but a limited workspace on the other hand. Moreover, this method avoids any dynamic singularities associated with the uncontrolled attitude of the base-spacecraft, thus, allowing the end effector's orientation and position to be a unique function of the manipulator's joint angles independently of the history of the joint's trajectory [5]. On the other contrary, in the Free-Floating approach, the AOCS is turned off to conserve on-board fuel. This means that the position and attitude of the base-spacecraft are not actively controlled during the capturing motion of the manipulator. As a result, the base-spacecraft will in response move freely to the manipulator's motion, hence, introducing holonomic and non-holonomic kinematic constraints [5]. Moreover, free-floating systems are characterized by unpredictable dynamic singularities in the workspace of the manipulator, as a result of changing the attitude of the base-spacecraft at which point they become unstable [7]. Dynamic singularity is a function of both the manipulator's kinematics as well as dynamic properties, such as the masses and inertia of both the base-spacecraft and the manipulator. Therefore, the attitude of the spacecraft becomes dependent on the path history of the manipulator due to its non-holonomic nature. Moreover, if the attitude of the base-spacecraft is not being controlled, the reachable path independent workspace by the manipulator becomes significantly smaller than the constrained workspace available to the free-flying approach [8].

When fuel expenditure is to be minimized, a combination of these approaches should be employed during different phases of operation [9]. Thus, a new mode of operation, called the Controlled-Floating approach, introduced in [10] is used in this study. In this approach, the base-spacecraft is allowed to move and rotate in a controlled manner to match translational and angular rates with the target spacecraft, hence making it easier for the end-effector of the manipulator to perform different on-orbit operations. This method has the benefits of both Free-Flying and Fee-Floating systems, i.e., it minimizes the fuel consumption, offers extra redundancy and doesn't encounter any dynamic singularities in the workspace. Moreover, this approach offers un-limited workspace which is not possible with the traditional approaches. In conclusion, Table 1 gives a breakdown of the Pros and Cons of each of the three approaches.

Table 1 Pros and Cons of different modes of operation for a space robot

	Pros	Cons
Free-Flying	Stabilized and Controlled base No dynamic singularities Similar to Earth-based manipulators Only Kinematic singularities	Excessive fuel consumption Restricted workspace Actuator saturation Restricted workspace
Free-Floating	No Fuel consumption	Base is allowed to move and rotate freely Kinematics affect the Dynamic properties Dynamic singularities occur in workspace Un-defined workspace Non-holonomic redundancy
Controlled-Floating	Optimum Performance Infinite Workspace Matching Linear and Angular rates No Dynamic singularities	High Complexity

2.2 Control Algorithms

The control of space robot is considered difficult for a number of factors. Their controller must be able to handle the difficult problems of compensating and accommodating for low resonance frequencies and non-linear actuator saturations [11]. Reliability policy for space development recommends the use of space qualified and reliable technologies and subsystem's parts, and are reluctant to introducing advanced and new technologies. Thus, the satellite attitude is best to be controlled by conventional Proportional- Derivative (PD) or Proportional-Integral-Derivative (PID) feedback controllers. Further, considering the applications of the space robot, it can be considered too risky to use the manipulator during close-proximity operations without controlling both the attitude and the position of the spacecraft to which it is mounted. This, however, requires a high level of reliability, accuracy and forces for a fully controlled spacecraft. Considering the efforts and the costs involved in the development of the mission, an uncontrolled spacecraft during extremely crucial missions seems to be inapplicable [12]. In general, a linear feedback attitude controller is sufficient on the satellite to maintain the attitude and provide stability for the system subjected to any environmental perturbations in space.

Although this paper is not focused on the flexural dynamics, it is worth noting that rigid body controllers such as the Computer Torque Controller (CTC), which consists of feed-forward linearization followed by a PID controller, will actively damp out the vibrations to some extent, therefore, improving the stability of the system. Alternatively, other control algorithms for the manipulator such as the optimal controllers or the adaptive techniques can be used, but the advantage of the CTC is that it provides robustness to compensate for any model uncertainties [8].

2.2.1 Feed-Forward Compensation

For space robots, the coupling reaction forces and moments that arise due to the manipulator's motion is tremendously larger than the most common environmental perturbations. Thus, the feedback controllers which depends on detecting the attitude error using the on-board sensors will not be effective on its own. Instead, a better solution is to use feed-forward compensation which anticipates for the manipulator's reactions [13]. By using feed-forward compensation, reaction forces and moments acting on the base-spacecraft due to the manipulator's motion may be computed directly from the dynamics of the manipulator and be feed-forward to the attitude control system of the spacecraft. RW, Control Moment Gyros (CMGs) and thrusters can then be used to counteract these coupling effects on the spacecraft's mounting. In addition, a standard attitude control algorithm may be used in parallel to maintain the spacecraft's attitude stabilized against any other environmental perturbations, as it is crucial for spacecraft's subsystems like solar cells, Antenna's and payload equipment to have a certain pointing accuracy.

Employing Feed-Forward compensation scheme to the control algorithm, stabilizes the position and attitude of the base-spacecraft and improves the dynamic stability of the space robot by a full order of magnitude over the Free-Floating approach. The Japanese ETS VII OOS experiment showed that the lack of attitude control while operating the manipulator on the servicer spacecraft led to many problems [14]. Therefore, it is essential to use active dedicated attitude control of the

base-spacecraft. This can be done by employing active three-axis attitude stabilization by non-fuel expending wheels, such as RWs, Momentum Wheels (MWs) or CMGs to compensate for these dynamic coupling effects.

2.2.2 PID Controller

Stabilizing a space robot with un-modeled uncertainties and external perturbations is a tedious task. In the literature, there are different methods such as the adaptive control [15], H_∞ control , fuzzy control [16], optimal control, and feedback linearization [17] to list a few. Although these non-linear robust control methods result in high performance and robustness, solving the associated Hamilton-Jacobi equation is often extremely complicated, and requires huge computational power; therefore, it makes the resulting controller hard to implement on the AOCS systems. On the contrary, PID controllers are known as the most widely used controllers in the industry with more than 90% of industrial systems in motion control, process control and aerospace systems use PID controllers [18]. The popularity of this controller is due to several factors like its simple structure, robustness to system's inertia matrix, understandable principles, simple implementation, specific physical meaning and adjustable frequency response measure such as the gain margin, phase margin and bandwidth frequencies. Moreover, multiple simple and complicated tuning algorithms have been proposed to design the optimal PID controller [19], or to improve the closed loop performance of the system such as the Ziegler–Nichols [20] and Åström-Hägglund phase margin [21] methods. However, implementing such tuning algorithms may not lead to an acceptable closed-loop response, particularly for dynamical systems with time varying coefficients [22]. Moreover, tuning techniques must be simple and applicable for a vast variety of processes [23], additionally, it is observed that the closed loop response is rather sensitive to parametric perturbations when such tuning rules are implemented [24].

Nevertheless, conventional PID controllers are not robust enough for various applications such as time-varying processes, large time delays, visible non-linearities and disturbance interactions [25]. Moreover, PID controllers with fixed gains cannot stabilize perfectly a non-linear system with uncertainties in terms of the model and parameters [26] and it suffers from a low convergence rate [27]. To overcome these limitations, PID controllers are introduced only as the 3rd and final stage of the control algorithm after employing feed-forward compensation and feed-forward linearization to decouple and linearize the non-linear space robot respectively.

2.2.3 LQR Controller

Linear-Quadratic-Regulators (LQR) controllers offer high efficiency controls that ensure both positioning accuracy and fuel optimization [28]. Moreover, they are widely used to control space systems. In [29], Yang proved the effectiveness of a quaternion-based LQR method for the design of non-linear AOCS of the spacecraft, demonstrating how the designed controller made the non-linear spacecraft system globally stable and optimized its performance. Another proof of LQR's effectiveness and reliability was given by Walker and Spencer [30]. Therefore, in this paper, the simulation results using the LQR controller as the 3rd stage of the control algorithm is presented and compared against its PID counterpart in terms of performance, robustness and required control action.

3 Dynamics and Kinematics of a Space Robot

Orbiting space robots are characterized by complex, extended structures, and are often modelled using the generalized multi-body dynamics. The payloads that the end-effector of the manipulator grasps are assumed to be attached to it and rigid. However, they increase the dynamic coupling effect due to increased mass and inertia of the arm, making its order of magnitude comparable to that of the spacecraft. Thus, the payloads and the manipulator are regarded as a multi-body system representing a kinematic tree of interconnected rigid bodies [31]. Any rotational motion of the bodies will produce a relative rotational and translational motion with respect to each other. The direct path approach was adopted, where determining the contribution of the motion of each body on its own to coefficient matrices of the overall mathematical model, therefore, describing the dynamics of the overall system. This approach is a vectoral path from the primary reference body, i.e. the base-spacecraft to the center of mass of each separate body, i.e. manipulator links, comprising the system. Robot dynamics is involved with relating the motion of the joints to the required joint torques to achieve certain trajectories. The required motor joint torques are computed to enforce precise trajectory tracking of the end-effector of the manipulator, describing its Cartesian motion. A typical 6 Degrees of Freedom (DoF) manipulator mounted onto a 6 DoF base-spacecraft generates a 12 DoF redundant space robot. The governing dynamical equations can be expressed as [10]:

$$\begin{bmatrix} F_{sc} \\ \tau_{sc} \\ \tau_m \end{bmatrix} = \begin{bmatrix} \mathbf{D_{sc}} & \mathbf{D_{sc.m}} \\ \mathbf{D_{sc.m}^T} & \mathbf{D_m} \end{bmatrix} \begin{bmatrix} \ddot{X} \\ \ddot{\theta} \end{bmatrix} + \begin{bmatrix} \mathbf{C_{sc}} & \mathbf{C_{sc.m}} \\ \mathbf{C_{sc.m}^T} & \mathbf{C_m} \end{bmatrix} \begin{bmatrix} \dot{X} \\ \dot{\theta} \end{bmatrix}, \tag{3.1}$$

where $\mathbf{D_{sc}}, \mathbf{D_{sc.m}}, \mathbf{D_m}$ represents the inertial acceleration terms and $\mathbf{C_{sc}}, \mathbf{C_{sc.m}}, \mathbf{C_m}$ represents the nonlinear Coriolis and Centrifugal force terms. $\mathbf{X}$ represents the state vector of the spacecraft while $\boldsymbol{\theta}$ represents the state vector of the manipulator:

$$X = [r_0 \quad \phi] = [x \quad y \quad z \quad \alpha \quad \beta \quad \gamma] \quad \text{and} \quad \theta = [\theta_1 \quad \theta_2 \quad \theta_3 \quad ... \quad \theta_n],$$

where r_0 is the relative position vector from the center of mass of the base-spacecraft to the center of mass of the target spacecraft, ϕ represent the Euler angles representing the rotation of the base-spacecraft with respect to the inertial frame and θ_i is rotation angle of the ith joint.

3.1 Dynamics of the base-spacecraft

For obtaining the dynamic model of the base-spacecraft, the terms $\boldsymbol{D_{sc}}$ and $\boldsymbol{C_{sc}}$, which represent the Inertial and the non-linear accelerations of the spacecraft respectively, and are represented as follows:

$$\mathbf{D_{sc}} = \begin{bmatrix} \mathbf{D_v} & \mathbf{D_{v\omega}} \\ \mathbf{D_{\omega v}} & \mathbf{D_\omega} \end{bmatrix} \qquad \mathbf{C_{sc}} = \begin{bmatrix} \mathbf{0} & \mathbf{C_{sc.v}} \\ \mathbf{0} & \mathbf{C_{sc.\omega}} \end{bmatrix}, \tag{3.2}$$

where the terms $\mathbf{D_v}, \mathbf{D_{v\omega}}, \mathbf{C_{sc.v}}$ are derived based on the conservation of the Linear momentum of the system, while $\mathbf{D_{\omega v}}, \mathbf{D_\omega}, \mathbf{C_{sc.\omega}}$ are based on the conservation of the angular momentum. Fig. 1 represents some basic parameters used to define the position vectors of different part of the overall system.
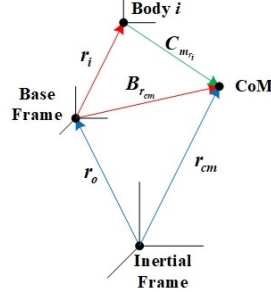
Fig. 1 Relative Position Vectors [10]

Here r_0 is position vector from the Inertial frame to the center of mass of the base-spacecraft, r_i is position vector of the CoM of the ith link to the center of mass of the base-spacecraft, $B_{r_{cm}}$ is position vector from the CoM of the base-spacecraft to the Com of the overall system, $C_{m_{r_i}}$ is position vector from the CoM of the ith link to the center of mass of the overall system and r_{cm} is the position vector from the Inertial frame to the CoM of the overall system. The total Inertia of the space robot can be defined as follow:

$$\mathbf{I_{tot}} = \mathbf{I_{sc}} - \mathrm{M_{sc}} \left[\boldsymbol{B_{r_{cm}}}\right]_\times \left[\boldsymbol{B_{r_{cm}}}\right]_\times + \sum_{i=1}^{n}(\mathbf{R_i^0} \mathbf{I_i} \mathbf{R_i^{0^T}} - \mathrm{m_i}[\boldsymbol{cm_{ri}}]_\times[\boldsymbol{cm_{ri}}]_\times) \quad (3.3)$$

where $\mathbf{I_{sc}}$ is the moment of inertia on the base-spacecraft at its center of mass, M_{sc} is the mass of the base-spacecraft, $\mathbf{I_i}$ is the inertia matrix of each link of the manipulator about its center of mass, m_i is the mass of the $\boldsymbol{i^{th}}$ link and $\mathbf{R_i^0}$ is the rotation transformation matrix to transform any vector from a frame attached to the ith link to the inertial frame (DH 4x4 matrix). Based on the Conservation of linear and angular momentum, the terms of equation (3.2) are:

$$\mathbf{D_v} = \mathrm{M_{tot}}\mathbf{E}, \ \ \mathbf{D_{v\omega}} = -\mathrm{M_{tot}}\left[\boldsymbol{B_{r_{cm}}}\right]_\times \mathbf{R_\omega}, \ \ \mathbf{D_{\omega v}} = \mathrm{M_{tot}}\left[\boldsymbol{B_{r_{cm}}}\right]_\times, \ \ \mathbf{D_\omega} = \mathbf{AR_\omega} \quad (3.4)$$

$$\mathbf{C_{sc_v}} = -\mathrm{M_{tot}}\left[\boldsymbol{B_{r_{cm}}}\right]_\times \dot{\mathbf{R}}_\omega - \mathrm{M_{tot}}[\boldsymbol{\omega_{sc}}]_\times \left[\boldsymbol{B_{r_{cm}}}\right]_\times \mathbf{R_\omega}, \ \ \mathbf{C_{sc_\omega}} = \mathbf{A\dot{R}_\omega} + [\boldsymbol{\omega_{sc}}]_\times \mathbf{BR_\omega} \quad (3.5)$$

$$\text{As,} \ \ \mathbf{A} = \mathbf{I_{sc}} - (\mathrm{M_{tot}} + \mathrm{M_{sc}})\left[\boldsymbol{B_{r_{cm}}}\right]_\times \left[\boldsymbol{B_{r_{cm}}}\right]_\times + \sum_{i=1}^{n}\left(\mathbf{R_i^0} \mathbf{I_i} \mathbf{R_i^{0^T}} - \mathrm{m_i}[\boldsymbol{cm_{ri}}]_\times[\boldsymbol{cm_{ri}}]_\times\right) \quad (3.6)$$

$$\mathbf{B} = \mathbf{I_{sc}} - \mathrm{M_{sc}} \left[\boldsymbol{B_{r_{cm}}}\right]_\times \left[\boldsymbol{B_{r_{cm}}}\right]_\times + \sum_{i=1}^{n}\left(\mathbf{R_i^0} \mathbf{I_i} \mathbf{R_i^{0^T}} - \mathrm{m_i}[\boldsymbol{cm_{ri}}]_\times[\boldsymbol{cm_{ri}}]_\times\right) - \mathrm{M_{tot}}\left[\boldsymbol{B_{r_{cm}}}\right]_\times \quad (3.7)$$

Here $\mathbf{E}$ is the identity $\mathbb{R}^{3\times3}$ matrix and R_ω is the angular velocity matrix:

$$\mathbf{R_\omega} = \begin{bmatrix} 1 & 0 & -\sin\beta \\ 0 & \cos\alpha & \sin\alpha\cos\beta \\ 0 & -\sin\alpha & \cos\alpha\cos\beta \end{bmatrix} \quad (3.8)$$

3.2 Dynamics of the Robotic Manipulator

Based on the Lagrangian approach, it can be found that the $\mathbf{D_m}$ is expressed as:

$$\mathbf{D}_m(\boldsymbol{\theta}) = \sum_{i=1}^{n}\left(m_i \, \mathbf{J_{v_{m_i}}}(\boldsymbol{\theta})^T\mathbf{J_{v_{m_i}}}(\boldsymbol{\theta}) + \mathbf{J_{\omega_{m_i}}}(\boldsymbol{\theta})^T\mathbf{R_i} \, \mathbf{I_i} \, \mathbf{R_i^T} \, \mathbf{J_{\omega_{m_i}}}(\boldsymbol{\theta})\right) \quad (3.9)$$

where $\mathbf{J_{v_{m_i}}}(\boldsymbol{\theta})$ is the Translational Jacobian for the center of mass of the ith link and $\mathbf{J_{\omega_{m_i}}}(\boldsymbol{\theta})$ is the Rotational Jacobian for the center of mass of the ith link.

Prior to deriving the Jacobian matrix, one has to find the equation of the position of the end-effector with respect to the inertial frame and the total Jacobian of the system to decouple it into the spacecraft and manipulator Jacobian matrices [10].
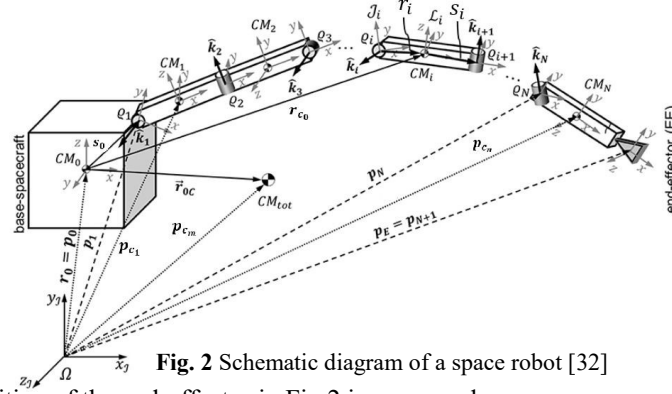
Fig. 2 Schematic diagram of a space robot [32]

The position of the end-effector in Fig 2 is expressed as:

$$P_e = r_{c_0} + \mathbf{R_0}\, S_0 + \sum_{i=1}^n \mathbf{R_i}\, L_i \tag{3.10}$$

where,

$$\mathbf{R_i} = \prod_{i=0}^n \mathbf{R_i^0} \tag{3.11}$$

P_e is the position vector of the end-effector, $\mathbf{R_0}$ is the rotation matrix of the base spacecraft with respect to the inertial frame, L_i is the vector from the ith joint to the $(i+1)^{th}$ joint, r_i is the distance from CoM of ith link to the preceding joint in the inertial frame and s_i is distance from CoM of ith link to the subsequently joint in the inertial frame. The translational and rotational Jacobian for the CoM of the ith link can be expressed as follows:

$$\mathbf{J_{v_{m_i}}} = \sum_{j=1}^i \left[\sum_{k=1}^j \frac{\partial \mathbf{R_j}}{\partial \theta_k} r_j + \sum_{k=1}^{j-1} \frac{\partial \mathbf{R_{j-1}}}{\partial \theta_k} s_{j-1} \right], \quad \mathbf{J_{\omega_{m_i}}} = \sum_{j=1}^i \mathbf{R_{j-1}^0}\, \widehat{k} \tag{3.12}$$

Accordingly, the $\mathbf{C_m}$ matrix can be found as,

$$\mathbf{C_m}(\boldsymbol{\theta}, \dot{\boldsymbol{\theta}}) = \begin{bmatrix} c_{11} & c_{12} & \cdots & c_{1n} \\ c_{21} & c_{22} & \cdots & c_{2n} \\ \vdots & \vdots & \cdots & \vdots \\ c_{n1} & c_{n2} & \cdots & c_{nn} \end{bmatrix}, c_{kj} = \sum_{i=1}^n c_{ijk}\, \dot{\theta}_i = \frac{1}{2}\sum_{i=1}^n \left[\frac{\partial d_{kj}}{\partial \theta_i} + \frac{\partial d_{ki}}{\partial \theta_j} - \frac{\partial d_{ij}}{\partial \theta_k} \right] \dot{\theta}_i \tag{3.13}$$

3.3 Dynamic Coupling between Manipulator and Base-Spacecraft

The dynamic coupling is referred to the relative forces and moments generated from the motion of the manipulator and applied on the base spacecraft, which causes the attitude to change. Modelling the dynamic coupling is based on the conservation of relative Linear and Angular momentum of the Manipulator. In order to find the dynamic coupling matrix $\mathbf{D_{sc.m}}$ and $\mathbf{C_{sc.m}}$, one has to compute the embedded matrices $\mathbf{D_{vm}}$, $\mathbf{D_{\omega m}}$, $\mathbf{C_{vm}}$ and $\mathbf{C_{\omega m}}$ from relative linear and angular momentum where:

$$\mathbf{D_{sc.m}} = \begin{bmatrix} \mathbf{D_{vm}} \\ \mathbf{D_{\omega m}} \end{bmatrix} \quad \text{and} \quad \mathbf{C_{sc.m}} = \begin{bmatrix} \mathbf{C_{vm}} \\ \mathbf{C_{\omega m}} \end{bmatrix} \tag{3.14}$$

Based on the conservation of relative linear momentum, it can be found that:

$$\mathbf{D_{vm}} = \sum_{i=1}^n m_i\, \mathbf{J_{T_i}}, \quad \mathbf{C_{vm}} = \sum_{i=1}^n m_i\, \mathbf{J_{T_i}} \tag{3.15}$$

where $\mathbf{J_{T_i}}$ is the relative linear translational Jacobian and can be expressed as:

$$\mathbf{J_{T_i}} = \sum_{j=1}^i \left[\sum_{k=1}^j \frac{\partial \mathbf{R_j}}{\partial \theta_k} r_j + \sum_{k=1}^{j-1} \frac{\partial \mathbf{R_{j-1}}}{\partial \theta_k} s_{j-1} \right] \tag{3.16}$$

Based on the conservation of relative angular momentum, it can be found that:

$$\mathbf{D_{\omega m}} = \sum_{i=1}^{n} \left(\mathbf{R_i^0 I_i R_i^{0^T}} \mathbf{J_{\omega_i}} + \mathrm{m_i} \left[\boldsymbol{p_{c_i}} \right]_{\times} \mathbf{J_{T_i}} \right), \mathbf{C_{\omega m}} = \sum_{i=1}^{n} \left(\mathbf{R_i^0 I_i R_i^{0^T}} \dot{\mathbf{J}}_{\omega_i} + \mathrm{m_i} \left[\boldsymbol{p_{c_i}} \right]_{\times} \dot{\mathbf{J}}_{T_i} \right) \quad (3.17)$$

where $\boldsymbol{p_{ci}}$ is the position vector of CM of ith link with respect to inertia frame and $\boldsymbol{J}_{\omega_i}$ is the angular velocity Jacobian of the ith link. Therefore, the final inertial acceleration matrix **D** and the centrifugal and Coriolis acceleration matrix **C** are:

$$\mathbf{D} = \begin{bmatrix} \mathbf{D_v} & \mathbf{D_{v\omega}} & \mathbf{D_{vm}} \\ \mathbf{D_{v\omega}^T} & \mathbf{D_\omega} & \mathbf{D_{\omega m}} \\ \mathbf{D_{vm}^T} & \mathbf{D_{\omega m}^T} & \mathbf{D_m} \end{bmatrix}, \qquad \mathbf{C} = \begin{bmatrix} \mathbf{0} & \mathbf{C_{sc.v}} & \mathbf{C_{vm}} \\ \mathbf{0} & \mathbf{C_{sc.\omega}} & \mathbf{C_{\omega m}} \\ \mathbf{C_{vm}^T} & \mathbf{C_{\omega m}^T} & \mathbf{C_m} \end{bmatrix} \qquad (3.18)$$

3.4 Forward and Inverse Kinematics for a Space Robot

By referring to equation (3.12) and Fig. 2, the forward kinematics for the end-effector of the manipulator can be expressed as: $\dot{\boldsymbol{P}}_e = [\mathbf{J_{v_{sc}}} \quad \mathbf{J_{v_m}}] \begin{bmatrix} \dot{X} \\ \dot{\boldsymbol{\theta}} \end{bmatrix}$ (3.19)

Through using the pseudo inverse, the inverse kinematics can be expressed as:

$$\dot{\boldsymbol{\theta}} = \left(\mathbf{J_{v_m}^T J_{v_m}} \right)^{-1} \mathbf{J_{v_m}^T} (\dot{\boldsymbol{P}}_e - \mathbf{J_{v_{sc}}} \dot{X}) \qquad (3.20)$$

As, $\qquad \mathbf{J_{v_{e_{sc}}}} = \begin{bmatrix} \mathbf{E} & \mathbf{J_{v_{sc}}'} \end{bmatrix}, \quad \mathbf{J_{v_{e_{sc}}}'} = \dfrac{\partial \mathbf{R_0}}{\partial \phi} \boldsymbol{S_0} + \sum_{i=1}^{n} \dfrac{\partial \mathbf{R_i}}{\partial \phi} \boldsymbol{L_i} \qquad (3.21)$

$$\mathbf{J_{v_{e_m}}} = \sum_{i=1}^{n} \sum_{k=1}^{i} \left(\dfrac{\partial \mathbf{R_i}}{\partial \theta_k} \right) \boldsymbol{L_i} \qquad (3.22)$$

where $\boldsymbol{\phi}$ is the Euler angles of the base-spacecraft, $\mathbf{R_0}$ is the axes transformation matrix for the base-spacecraft using Yaw, Pitch and Roll (3-2-1) rotation sequence and is given by,

$$\mathbf{R_0} = \begin{bmatrix} \cos\phi \cos\theta & \cos\phi \sin\theta \sin\psi - \sin\phi \cos\psi & \cos\phi \sin\theta \cos\psi + \sin\phi \sin\psi \\ \sin\phi \cos\theta & \sin\phi \sin\theta \sin\psi + \cos\phi \cos\psi & \sin\phi \sin\theta \cos\psi - \cos\phi \sin\psi \\ -\sin\theta & \cos\theta \sin\psi & \cos\theta \cos\psi \end{bmatrix} \quad (3.23)$$

Fig. 3 shows the closed-loop simulation of the non-linear dynamic model discussed in Section 3. Here the base-spacecraft is controlled by the AOCS controller to reach the required relative linear and angular rates to match the target spacecraft using feedback from the Inertial sensors. On the other hand, the manipulator is being controlled by the arm controller to enable its end-effector to track the required trajectory.
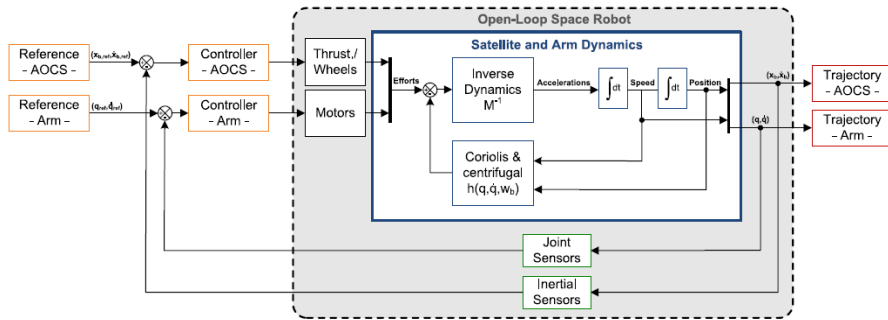

**Fig.** 3 Simulation of the mathematical model for the space robot [6]

4 Space Environment and Parametric Uncertainty

4.1 Environmental Perturbations

As aforementioned in Sec. 1, the space robot will be subjected to environmental perturbations due to the micro-gravity environment in space; this is mainly due to Gravity Gradient, Aerodynamic Drag, Solar Pressure and Residual Magnetic disturbances. Disturbances observed on the previous missions had a sinusoidal behavior with some fluctuations of a varying frequencies. Moreover, these perturbations can be influenced by multiple factors, mainly the orbit parameters of the space robot and the state of the solar activities and magnetic storms. Previous data shows that the maximum value of these perturbations combined is of the order of magnitude $10^{-5} \, Nm$, however, these data were only correlated to normal satellites [33]. Nevertheless, a space robot may encounter different order of magnitude of these perturbations due to their bigger size and its robotic manipulator, which acts as a gravity boom during operation, therefore increasing the effects of the gravity gradient tremendously. In fact, data from the Japanese spacecraft ETS VII that was equipped with a 2m long robotic arm showed that these disturbances are significantly larger than that experienced by a typical spacecraft. The order of magnitude of perturbations experienced by the ETS VII was in the order of $\sim 10^{-6} \rightarrow 10^{-3} \, Nm$, which is 100 times bigger than what the typical spacecraft encounters [33]. Therefore, based on these data, the external disturbances used in this paper for simulations are sinusoidal waves with a Gaussian random noise of zero mean. In addition, the magnitude of the disturbances used here are 3 order of magnitudes higher than the ones observed in previous space missions. This allows for a good margin of safety and also testing the limits and robustness of the proposed control algorithms against these huge disturbances. Table 2 gives a breakdown of the external disturbances used and their corresponding parameters. The characteristics of the disturbances acting on the thrusters are shown in Fig. 4. Furthermore, same disturbances are imposed on the reaction wheels and joint motors but with different order of magnitude.

Table 2 External Environmental Perturbations used in simulation

	Sinusoidal		Gaussian Random Noises	
	Magnitude	**Frequency**	**Mean**	**Standard Deviation**
Disturbance Forces on Thrusters	0.8	$2 \, rad/s$	0	0.1
Disturbance Moments on Reaction Wheels	0.4	$2 \, rad/s$	0	0.08
Disturbance Moments on Joint Motors	0.1	$2 \, rad/s$	0	0.03
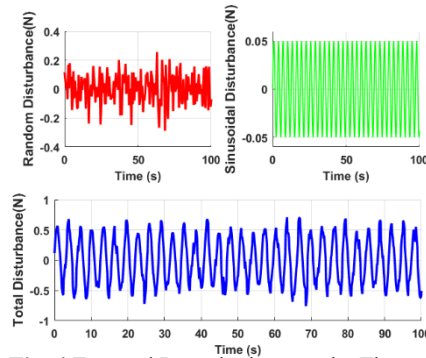
Fig. 4 External Perturbations on the Thrusters

4.1 Parametric Uncertainty

In practical robotic systems, the parameters of the system cannot be *a priori* known exactly, for example, the load may vary while performing various operations; thus, varying the friction coefficient in different configurations. Moreover, some neglected non-linearity, such as backlash, may introduce disturbances to the control action. Therefore, it is crucial to consider the effects of internal parametric uncertainty on the model [34]. Internal disturbances may be caused by any uncertainties in the **D** or **C** matrices due to any un-modeled parametric changes in the system. For example, any uncertainty in computing the actual fuel consumption may result in major internal disturbances that will affect the performance of the system [34]. Accordingly, the additional internal disturbances imposed on the system can be written as:

$$\begin{bmatrix} \Delta F_{sc} \\ \Delta \tau_{sc} \\ \Delta \tau_m \end{bmatrix} = \begin{bmatrix} \Delta \mathbf{D}_{sc} & \Delta \mathbf{D}_{sc.m} \\ \Delta \mathbf{D}_{sc.m}^{\mathrm{T}} & \Delta \mathbf{D}_m \end{bmatrix} \begin{bmatrix} \ddot{X} \\ \ddot{\theta} \end{bmatrix} + \begin{bmatrix} \Delta \mathbf{C}_{sc} & \Delta \mathbf{C}_{sc.m} \\ \Delta \mathbf{C}_{sc.m}^{\mathrm{T}} & \Delta \mathbf{C}_m \end{bmatrix} \begin{bmatrix} \dot{X} \\ \dot{\theta} \end{bmatrix} \quad (4.1)$$

In this paper, for simulation purpose, the internal disturbance due to the uncertainty in fuel consumption was considered and this will in turn produce a change in the $\mathbf{D}_{sc}$ and $\mathbf{C}_{sc}$ matrices. Therefore, it produces a force and moment that will alter the linear and angular motion of the base-spacecraft. Thus, the above equation can be re-written as:

$$\begin{bmatrix} \Delta F_{sc} \\ \Delta \tau_{Sc} \end{bmatrix} = \Delta \mathbf{D}_{sc} \, \ddot{X} + \Delta \mathbf{C}_{sc} \, \dot{X} \quad (4.2)$$

Based on equation (4.2), the dependency of these internal disturbance on the states of the system which are changed by the control algorithm is apparent. Therefore, each simulation is going to have different internal disturbances imposed. Results in Fig. 5 are obtained from the Control-Floating mode simulation over 100 s. It shows the effects of the uncertainty in fuel consumption, which accordingly will change the mass of the spacecraft and in turn produce internal disturbances on the system. It can be seen that these disturbances also follow a cyclic behavior due to the imposed external disturbance on the system as discussed in Sec. 4.1.
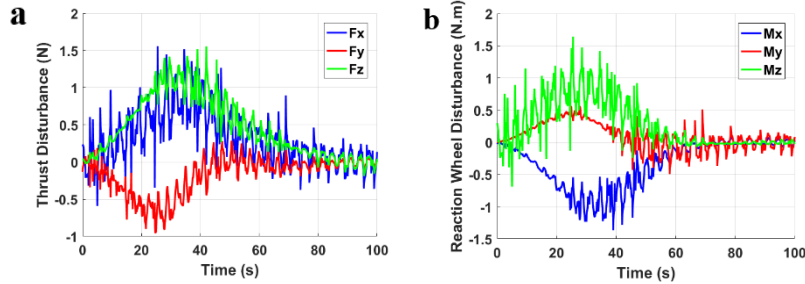

Fig. 5 Internal Disturbances due to parametric uncertainties: (a) on Thrusters, (b) on RW

5 Control System Design for a Space Robot

In this section, a 3-stage control algorithm is presented for the space robot. The first stage would be feed-forward compensation to decouple the space robot system into a 6 DoF robotic manipulator and a 6 DoF base-spacecraft as well as compensating

for the dynamic coupling reaction forces and moments between the two decoupled systems. The second stage would be feed-forward linearization using a non-linear controller to linearize both decoupled non-linear systems. The third and the final stage of control will be to design a linear PID or LQR controller for the linearized de-coupled systems. The step-by-step process for designing the controller is described here below:

5.1 Feed-Forward Compensation

As stated in Section 2.2.1, to decouple the system, feed-forward compensation should be used to mitigate the effects of the $\mathbf{D}_{sc.m}$ and $\mathbf{C}_{sc.m}$ terms, as follows:

$$\begin{bmatrix} F_{sc_{FFC}} \\ \tau_{sc_{FFC}} \\ \tau_{m_{FFC}} \end{bmatrix} = \begin{bmatrix} \mathbf{0} & \mathbf{D}_{sc.m} \\ \mathbf{D}_{sc.m}^{\mathbf{T}} & \mathbf{0} \end{bmatrix} \begin{bmatrix} \ddot{X} \\ \ddot{\theta} \end{bmatrix} + \begin{bmatrix} \mathbf{0} & \mathbf{C}_{sc.m} \\ \mathbf{C}_{sc.m}^{\mathbf{T}} & \mathbf{0} \end{bmatrix} \begin{bmatrix} \dot{X} \\ \dot{\theta} \end{bmatrix} \qquad (5.1)$$

Hence, after applying the feed-forward compensation, the 12-DoF space robot system is decoupled into a 6 DoF base-spacecraft and a 6 DoF robotic manipulator. This decoupled system can be as follows:

$$\begin{bmatrix} F_{sc} \\ \tau_{sc} \\ \tau_m \end{bmatrix} = \begin{bmatrix} \mathbf{D}_{sc} & \mathbf{0} \\ \mathbf{0} & \mathbf{D}_m \end{bmatrix} \begin{bmatrix} \ddot{X} \\ \ddot{\theta} \end{bmatrix} + \begin{bmatrix} \mathbf{C}_{sc} & \mathbf{0} \\ \mathbf{0} & \mathbf{C}_m \end{bmatrix} \begin{bmatrix} \dot{X} \\ \dot{\theta} \end{bmatrix} \qquad (5.2)$$

As seen from equation (5.2), the mutual dynamic coupling is eliminated by removing the terms $\mathbf{D}_{sc.m}$ and $\mathbf{C}_{sc.m}$ from the dynamics equation.

5.2 Feed-Forward Linearization

The dynamic model obtained using feed-forward compensation in equation (5.2) is still very complex, extremely dynamic and non-linear in nature. Hence, a linear PID or LQR controller cannot guarantee stability of the closed loop system. Therefore, to solve this issue, the feed-forward linearization technique is applied after the feed-forward compensation process to linearize the decoupled systems. This allows the use of a LQR or PID controller in the final stage. To do so, the control law for feed-forward linearization is written as follows:

$$\begin{bmatrix} F_{sc_{FFL}} \\ \tau_{sc_{FFL}} \\ \tau_{m_{FFL}} \end{bmatrix} = \begin{bmatrix} \mathbf{D}_{sc} & \mathbf{0} \\ \mathbf{0} & \mathbf{D}_m \end{bmatrix} \begin{bmatrix} F_{sc_{Linear}} \\ \tau_{sc_{Linear}} \\ \tau_{m_{Linear}} \end{bmatrix} + \begin{bmatrix} \mathbf{C}_{sc} & \mathbf{0} \\ \mathbf{0} & \mathbf{C}_m \end{bmatrix} \begin{bmatrix} \dot{X} \\ \dot{\theta} \end{bmatrix} \qquad (5.3)$$

Using equation (5.3) in (5.2):

$$\begin{bmatrix} F_{sc_{Linear}} \\ \tau_{sc_{Linear}} \\ \tau_{m_{Linear}} \end{bmatrix} = \begin{bmatrix} \ddot{X} \\ \ddot{\theta} \end{bmatrix} \qquad (5.4)$$

Therefore, as seen from equation (5.4), feed-forward linearization results in a simple, decoupled-linear system that can be further controlled using conventional LQR or PID controllers.

5.3 PID Controller

As discussed in Section 2.2.2, conventional PID controllers are not the best choice when it comes to controlling a space robot due to its high complexity, non-linearity and limited robustness to the aforementioned external perturbations and model uncertainties. Thus, the PID controller will be used only in the final stage of the three-stage control algorithm presented. In addition, this staging method allows tuning

the gains of the PID controller using the characteristic equation of the linearized - decoupled systems, therefore, gaining much better performance as a result of choosing accurate gain values. The PID linear controller which represents the third stage of the control algorithm can be expressed as:

$$\begin{bmatrix} F_{scLinear} \\ \tau_{scLinear} \\ \tau_{mLinear} \end{bmatrix} = \begin{bmatrix} \ddot{X}_{Desired} \\ \ddot{\theta}_{Desired} \end{bmatrix} + K_p \begin{bmatrix} X_{Desired} - X \\ \theta_{Desired} - \theta \end{bmatrix} + K_d \begin{bmatrix} \dot{X}_{Desired} - \dot{X} \\ \dot{\theta}_{Desired} - \dot{\theta} \end{bmatrix} + K_i \int \begin{bmatrix} X_{Desired} - X \\ \theta_{Desired} - \theta \end{bmatrix} \quad (5.5)$$
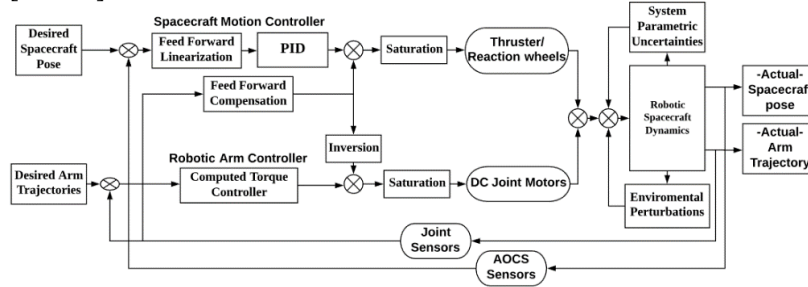

Fig. 6 Control scheme using the PID as a final stage controller

Fig. 6 shows the implementation of the 3-stage control algorithm with a PID controller as its final stage. It shows the feed-forward compensation scheme to eliminate the dynamic coupling reactions that are computed based on the reading of the joint sensors of the manipulator and it is fed-forward, in real-time, to the spacecraft motion controller so it counteracts these effects. Furthermore, saturation blocks are added to limit the control output within the practical limits of the actuation system on-board the spacecraft.

5.4 LQR Controller

The definition of the LQR control law requires the usage of state feedback gain whose design is based on the trade-off between the transient performance and control effort. Thus, the optimal control approach [35] to this trade-off is to define and minimize the cost function. Furthermore, since the robot generally has to reach a non-zero target position and attitude, a non-zero set point optimal control [36] has been considered. This enables the controller to follow a desired trajectory by shifting the actual state $x(t) = [X \, \theta]$ by a desired quantity x_d, obtaining the error, defined as:

$$x_e(t) = x_d(t) - x(t) \quad (5.6)$$

First, the procedure of solving the optimal control problem using the method of calculus of variations is developed. Thus, the control action $u(t)$ that stabilizes the closed loop system over a fixed time t_f and at the same time minimizes the cost function is given as:

$$J = \int_0^{t_f} x(t)^T Q \, x(t) + u(t)^T R u(t) dt \quad (5.7)$$

As shown in equation (5.7), the cost function is dependent on two terms, the first penalizes the variation of the states from the desired ones, while the second penalizes the use of excessive control action to control the system. Moreover, the weighting of these terms is controlled by the weighting matrices Q and R respectively. In the above terminology, $u(t)$ is the state feedback control law, resulting from the quadratic performance index optimization subjected to the state equations.

$\mathbf{Q}$ is a positive semi definite state weighting matrix, and $\mathbf{R}$ is the control weighting matrix that also has to be positive definite [37]. Therefore, the control law is written as:
$$\boldsymbol{u(t)} = \mathbf{K}\,\boldsymbol{x_{error}(t)} \tag{5.8}$$
where $\mathbf{K}$ is the state feed-back gain and can be found from:
$$\mathbf{K} = -\mathbf{R}^{-1}\mathbf{B}^{\mathbf{T}}\mathbf{P} \tag{5.9}$$
and $\mathbf{P}$ is the solution of the Algebraic Riccati equation (ARE)
$$\mathbf{A}^{\mathbf{T}}\mathbf{P} + \mathbf{P}\mathbf{A} - \mathbf{P}\mathbf{B}\mathbf{R}^{-1}\mathbf{B}^{\mathbf{T}}\mathbf{P} + \mathbf{Q} = \mathbf{0} \tag{5.10}$$

It is observed that an arbitrarily rapid reduction in the states of the system can be achieved at the expense of a corresponding increase in the control action that can be impossible to implement in practical situations. Moreover, an arbitrarily large reduction in control action may cause a significant elevation of the state and deviation from the desired set points, resulting in an undesirable situation in the attitude control process [38]. As a result, the selection of the gains of the Lyapunov control law and the weighting matrices of the LQR is an extremely laborious process. Thus, a reasonable choice of $\mathbf{Q}$ and $\mathbf{R}$ makes the closed-loop system acquire stable performance, while limiting the control action and minimizing fuel expenditure. However, in simulations the choices of the elements of the $\mathbf{Q}$ and $\mathbf{R}$ matrices was based on the diagonal weighting method, and verifying which values best meet the performance criteria such as overshot, maximum control energy and settling time, thus, reflecting a better performance of the system. Similar to the PID controller, Fig. 7 shows the implementation of the LQR controller as a final stage to maintain the stability of the space robot.
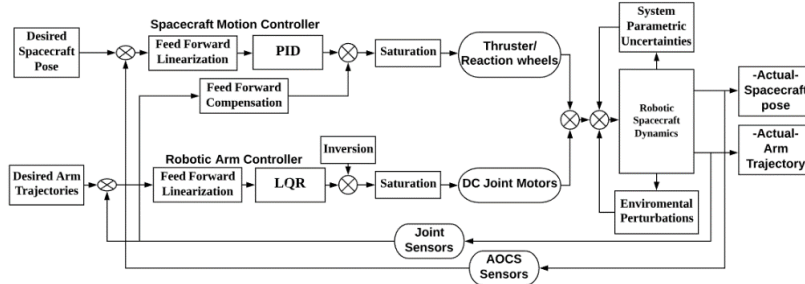

Fig. 7 Control scheme using the LQR as a final stage.

6 Simulations and Discussion

In this section, the performance and robustness of the PID controller is compared against its LQR counterpart for the controlled-floating space robot. The simulations took into account the presence of extreme external disturbances, internal fuel consumption and parametric uncertainties imposed on the system. A fifth order polynomial function is used to generate smooth trajectories between different set points for both the arm and the base-spacecraft. Additionally, the control action required from the on-board actuation systems is limited to $1 \rightarrow 5\ N$ for thrusters (like cold or hot gas thrusters) and up to $2\ N.m$ for RWs [39]. Since this paper is focused on the close-range approach with the target spacecraft, the orbital parameters are not relevant. Table 3 shows the parameters of the spacecraft, while a standard UR10

robotic arm [40] was used in the simulations.

**Table 3** base-spacecraft specifications

Mass [kg]	Length [m]	Width [m]	Height [m]	Principal Moments of Inertia [$kg\,m^2$]
200	1	1	1	[40,40,40]

6.1 PID Results

Simulation results using the PID controller in the Controlled-Floating approach are shown below. Fig. 8a shows the resulting 3D trajectory tracking graph for the end-effector of the manipulator. The PID controller was able to maintain perfect tracking of the desired trajectory without any cross-track errors or fluctuations along the path. Fig. 8b and 8c shows the actual relative position and attitude trajectories being followed by the base-spacecraft to attain the orientation and position with respect to the target whilst maintaining $1m$ distance to avoid any collisions. However, Fig. 8c shows some small fluctuations in ϕ till the steady state value is reached. On the other hand, Fig 9a shows some minor fluctuations of 2° on the 6th joint of the manipulator, which is a very reasonable accuracy for some missions. It is important to recall that these simulated results are for extreme environmental disturbances but under realistic micro-gravity environment, these responses will be much smoother and accurate; nevertheless, the extreme cases are considered here to test the limits of the control algorithms used. As seen in Fig. 9b, not only the PID controller was able to achieve perfect tracking, but also was able to achieve that under 1 N saturation limit on the thrusters. Therefore, it minimizes fuel consumption and this control effort is a small value compared to the capabilities of modern thrusters, which can reach $5N$. Moreover, Fig. 9c and d shows the saturation of the torque of the reaction wheels and joint motors at $1\,N.m$ to match the restrictions on power consumption for most commercial spacecraft.
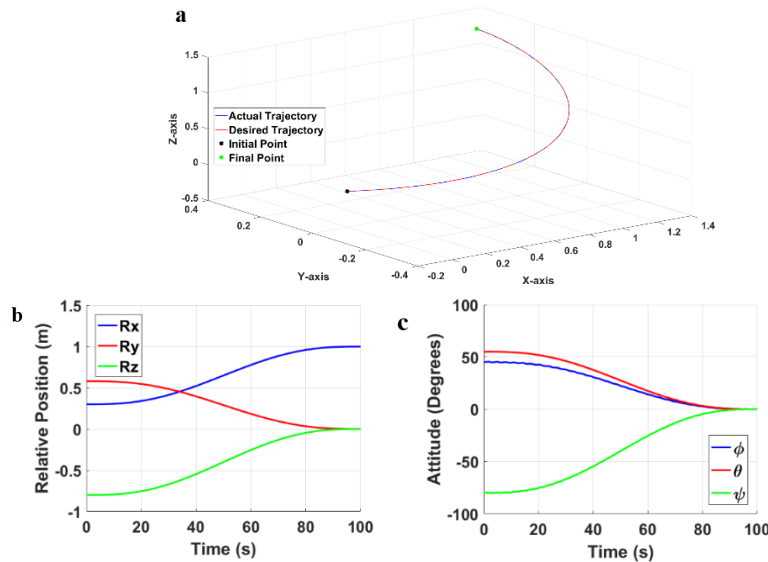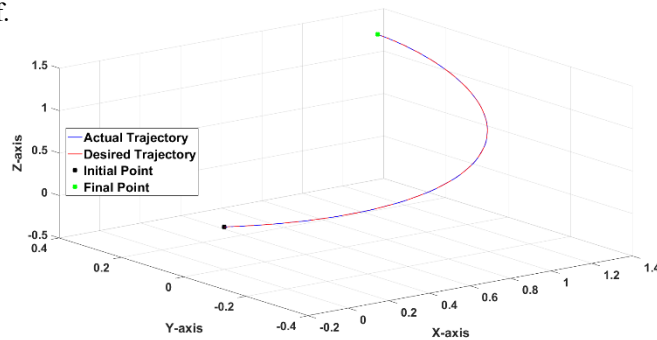

Fig. 8 Simulation Results for PID: (a) Trajectory Plot - (b) Relative position - (c) Relative attitude
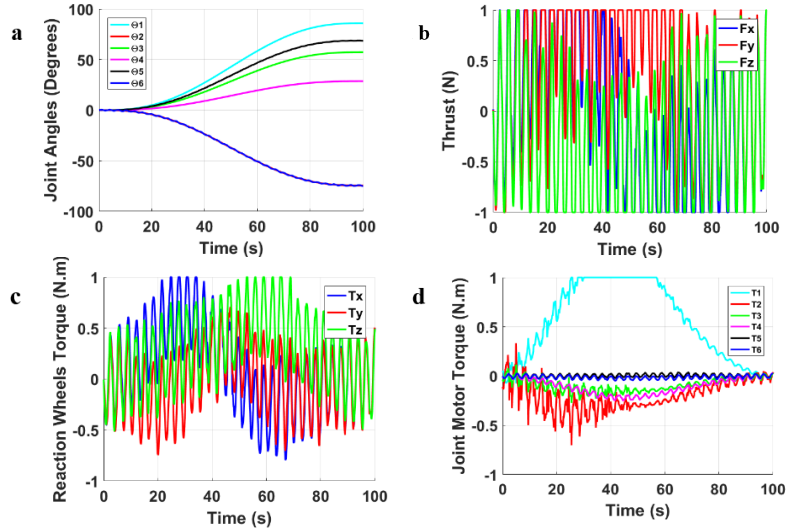
Fig. 9 Simulation Results for PID: (a) joint angles - (b) Thrusters force - (c) Reaction Wheels control Toques - (d) Joint Torques

6.2 LQR Results

For the LQR controller, Fig.10a shows the actual trajectory tracking of the end-effector of the robotic arm. By comparing Fig. 8a and 10a, it can be seen that the LQR controller was able to achieve excellent trajectory tracking like its PID counterpart. Nevertheless, the LQR controller was able to maintain a low fluctuation for the relative attitude, therefore, assuring a more stabilized motion. Moreover, it kept a slightly lower cyclic deviations on the 6th manipulator's joint as seen in Fig. 11c with a deviation less than 1°, thus, can be used for more accurate operation for the end effector. Although the LQR provided a slightly better performance with higher stability and accuracy, it required more control effort (see Fig. 11d), where the minimum saturation limit for operating the LQR controller was 1.5 N. Moreover, the control effort out produced by reaction wheels increased by 50% with a maximum value of 1.5 $N.m$ as shown in Fig. 11e and a value of 1.5 $N.m$ on the joint motors in Fig. 11f.

Fig. 10 Trajectory Plot for the LQR
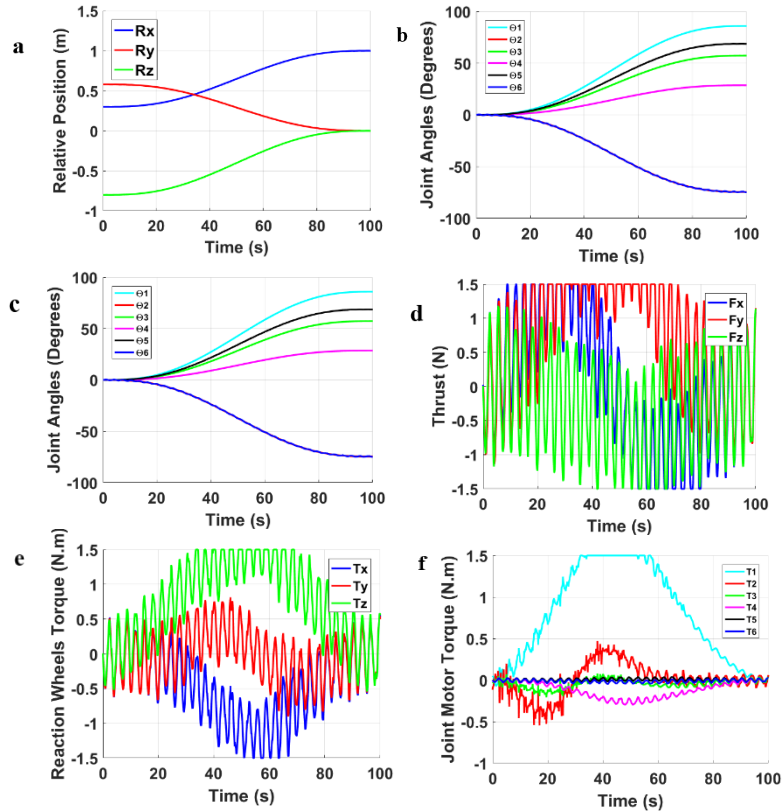
Fig. 11 Simulation Results for LQR: (a) relative position - (b) relative attitude - (c) joint angles - (d) Thrusters - (e) Reaction Wheels - (f) Joint Motors.

Table 4 Control algorithms execution time

Controller	Execution Time
PID	$0.5\ \mu s$
LQR	$0.9\ \mu s$
Feed-Forward Compensation	$0.9\ \mu s$
Feed-Forward Linearization	$16.5\ \mu s$
Over-all Execution Time	$21 - 22\ \mu s$

From the previous simulations, it is noticed that both PID and LQR controllers have a very similar performance. However, the LQR controller was able to offer a higher accuracy at the expense of about 50% more control effort, thus, higher fuel consumption. Therefore, depending on the mission requirements, PID or LQR should be chosen. Moreover, it should be noted that these trade-off analyses were conducted at extreme (3 orders of magnitude bigger than normal) environmental perturbations and internal disturbances. The reason for selecting such extreme values is that all previous data for the micro-gravity environment are applicable to normal spacecraft, therefore, the controllers developed for the space robot have to be robust enough to withstand the more vicious environmental and internal

perturbations due to its much more complex dynamics. Moreover, the simulation was converted into C code using Eclipse IDE for C/C++ and ran on i7-4710MQ CPU. Table 4 shows the execution time of each individual control block.

7 Conclusion

To undertake maintenance, repair or refueling of spacecraft, or assembly operations in space, the notion of a space robot is adopted, in which robotic manipulators are mounted on the base-spacecraft. Unlike Earth-based manipulators, the base of the space robot is not fixed in the inertial frame as a result of the dynamic coupling reactions during the motion of the manipulator. Hence, in order to develop control algorithms for such systems, it is crucial to consider the dynamic coupling effects and try to compensate for it. Moreover, the challenges facing a space robot over the fixed-based manipulators are presented, indicating the different modes of controlling a space robot and the pros and cons of each approach. Furthermore, the dynamic and kinematic modelling of a multi-DoF controlled-floating space robot in the close-range approach have been presented.

Control algorithms were developed where, Feed-Forward compensation was introduced to eliminate the dynamic coupling between the base-spacecraft; thus, decoupling the system into the base-spacecraft and the manipulator. Moreover, this is followed by a Feed-Forward linearization technique to linearize the non-linear decoupled systems, thus allowing the use of the linear LQR or PID controller as the last stage of the control algorithm. Closed loop simulations for the system were conducted, subjecting the space robot to extreme sinusoidal environmental perturbations with gaussian random white noises, as well as parametric uncertainty due to fuel expenditure. A trade-off analysis was conducted for both controllers based on their robustness to perturbations, accuracy in trajectory tracking, fluctuations in behavior and control effort required. Results showed that the LQR controller was able to offer slightly higher trajectory tracking performance with more robustness to environmental perturbations and 30% less fluctuations in the joint angles, relative attitude and velocities; however, it required 50% more control effort. Therefore, depending on the mission requirements, the AOCS designer could opt to choose between the slightly higher accuracy offered by the LQR controller or less fuel consumption offered by the PID controller.

As a next step, research into optimizing the path for the end-effector of the robotic arm as well as for the base-spacecraft, to minimize fuel consumption and achieve superior performance of the mission, is in progress. Additionally, other advanced concepts such as the kinematic and dynamic singularities along the path, applying real-time object avoidance algorithms to avoid collision with the target spacecraft is also under development.

References

1. A. Ellery, J. Kreisel, B. Sommer, "The case for robotic on-orbit servicing of spacecraft: Spacecraft reliability is a myth," *Acta Astronautica 63 (2008) 632–648*.
2. B. Barbee, J. Russel, S. Heatwole, et al. "A Guidance and Navigation Strategy for Rendezvous and Proximity Operations with a Noncooperative Spacecraft in

Geosynchronous Orbit," *The Journal of the Astronautical Sciences*, Vol. 58, No.3, July-September 2011, pp. 389-408.

3. Y. Xu, H. Shum, "Dynamic Control of A Space Robot System with No Thrust Jets Controlled Base," The Robotics Institute Carnegie Mellon University, Pittsburgh, PA 15213, August 1991.

4. T. Xia, S. L´eonard, A. Deguet, L. Whitcomb, P. Kazanzides, "Augmented Reality Environment with Virtual Fixtures for Robotic Telemanipulation in Space*," IEEE/RSJ International Conference on Intelligent Robots and Systems*, Vilamoura, Portugal, 7-12 Oct. 2012.

5. M. Shibli, "Modeling and Control of a Free-Flying Space Robot Interacting with a Target Satellite," Ph.D. dissertation, Mech. Eng, Concordia University, Dec. 2005

6. Dubanchet, Vincent and Saussié, David and Alazard, Daniel and Bérard, Caroline and Le Peuvedic, Catherine Modeling & control of a space robot for active debris removal. (2014) In: ESA GNC 2014 - 9th International ESA Conference on Guidance, navigation & Control Systems, 2 - 6 June 2014 (Porto, Portugal).

7. Papadopoulos, E. and Dubowsky, S. On dynamic singularities in the control of free-floating manipulators. *Trans. ASME, Dynamic Syst. and Control*, 1989, 15, 45–52.

8. A. Ellery, "An engineering approach to the dynamic control of space robotic on-orbit servicers," *Journal of Aerospace Engineering*, Volume: 218 issue: 2, pp. 79-98, February 1, 2004.

9. S. Ali, A. Moosavian, E. Papadopoulos, "Free-flying robots in space: an overview of dynamics modeling, planning and control," *Robotica*, volume 25, pp. 537–547. 2007.

10. A.Seddaou, C.Saaj. "Hα Controller for a Free-Flying Robotic Spacecraft," *Proc. 14th, International Symposium on Artificial Intelligence, Robotics and Automation in Space (i-SAIRAS 2018)*, Madrid, Spain, 4-6th June 2018

11. S. Dubowsky and E. Papadopoulos, "The Kinematics, Dynamics, and Control of Free-Flying and Free-Floating Space Robotic Systems," *IEEE Transactions on Robotics and Automation*. V. 9. No 5, 1993, pp. 531-543

12. E. Serpelloni, "Dynamics and Control of a Spacecraft-Manipulator System: Analysis, Simulation and Experiments," M.Sc. Thesis, Space Eng, Politecnico di Milano, 2011

13. K. Yoshida, "Practical Coordination Control Between Satellite Attitude and Manipulator Reaction Dynamics Based on Computed Momentum Concept," Proceedings of IEEE/RSJ International Conference on Intelligent Robots and Systems (IROS'94), Munich, Germany, 12-16 Sept. 1994.

14. Oda, M. "Attitude control experiments of a robot satellite", J. Spacecraft and Rockets, 2000, 37(6), 788–793.

15. M. Moradi, R. Esmaelzadeh, A. Ghasemi, "Adjustable adaptive fuzzy attitude control using nonlinear SISO structure of satellite dynamic," *Transaction of Japan Society for Aeronautical and Space Sciences, Volume 55 Issue 5,* pp. *265-273*, 2012

16. J.Kulkarni, M.Campbell, "An approach to magnetic Torque attitude control of satellites via H_∞ control for LTV system," *43rd IEEE Conference on Decision and Control*, 2004 , pp.273–277.

17. C.H. Cheng, S.L. Shu, P.J. Cheng, "Attitude control of a satellite using fuzzy controllers," *Expert Systems with Applications* 36 (2009) 6613–6620.

18. S.N. Singh, W. Yim, "Feedback linearization and solar pressure satellite attitude control," *IEEE Transactions on Aerospace and Electronic Systems 32* (1996) 732–741.

19. E. Almodaresi1, M. Bozorg, "K_p- stable regions in the space of PID controller coefficients," IET Control Theory & Applications, Volume 88, 2015 - Issue 3, pp. 653-662, April 2017.

20. Skogestad, S, "Probably the best simple PID tuning rules in the world," *AIChE Annual Meeting, Reno*, Nevada, 4-9th Nov,2001.

21. J.G. Ziegler, N.B. Nichols, "Optimum settings for automatic controllers," Annual Meeting, New York, N. Y., December 1-5, 1941, of the American Society of Mechanical Engineers.

22. K.J. Åström, T. Hägglund, "Advanced PID Control," *ISA-The Instrumentation, Systems and Automation Society*, Publisher: ISA, ISBN-13: 978-1556179426, 2006.

23. A. Dabiri , B.P. Moghaddam , J.A. Tenreiro Machado, "Optimal variable-order fractional PID controllers for dynamical systems," *Journal of Computational and Applied Mathematics* 339 (2018) 40–48

24. Astrom, K.J., Hagglund, T, "Automatic tuning of PID controllers" Instrumentation Systems and *Automation Society*, Volume 18, Issue 15, October 1985, Pages 205-210.

25. Ezzeddin M. Elarbi1, M.shaefi, "Disturbance Elimination using Self-tuning PID Controller for Spinning Satellite Types," *Int'l Journal of Computing, Communications & Instrumentation Engg. (IJCCIE)* Vol. 2, Issue 2 (2015) ISSN 2349-1469 EISSN 2349-1477

26. Morteza Moradi, "Self-tuning PID controller to three-axis stabilization of a satellite with unknown parameters," *International Journal of Non-Linear Mechanics 49* (2013) ,pp. 50–56.

27. You Li. Sun Zhaowei, Ye Dong, "Time Efficient Robust PID Plus Controller for Satellite Attitude Stabilization Control Considering Angular Velocity and Control Torque Constraint," *Journal of Aerospace Engineering, Volume 30 Issue 5 - September 2017.*

28. L. Guarnaccia, R. Bevilacqua, S. P. Pastorelli, "Suboptimal LQR-based spacecraft full motion control: Theory and experimentation," *Acta Astronautica* 122 (2016) 114–136.

29. Y.Yang, "Analytic LQR design for spacecraft control system based on quaternion model*," Journal of Aerospace Engineering 25(3):* pp. *448-453, July 2012*

30.   L. Walker, D. Spencer, "Automated proximity operations using image- based relative navigation," *26th Annual USU/AIAA Conference on Small Satellites*, 15th August 2012.

31. Z. Vafa, S. Dubbowsky, "The kinematics and dynamics of space manipulators: The virtual manipulator approach," *Int. J. Robotics Res*., vol. 9, no. 4, pp. 3-21, Aug. 1990.

32. Wilde M, Kwok Choon S, Grompone A and Romano M (2018) Equations of Motion of Free-Floating Spacecraft-Manipulator Systems: An Engineer's Tutorial. Front. Robot. AI 5:41. doi: 10.3389/frobt.2018.00041

33. X. Liu, H. Li, Y. Chen, "Dynamics and control of capture of a floating rigid body by a spacecraft robotic arm," *Multibody Syst Dyn*, March 2015, Volume 33, Issue 3, pp 315–332.

34. B. S. Chen, "A Non-Linear H∞ Control Design in Robotic Systems under parameter perturbation and external disturbance," *International Journal of Control*, Volume 59, 1994 - Issue 2, pp. 439-461, 11 Aug 2011.

35. I.M. Ross, "Control and Optimization: An Introduction to Principles and Applications," Electronic Edition, Naval Postgraduate School, Monterey, CA, December 2005.

36. H. Kwakernaak, R. Sivan, "Linear Optimal Control Systems," Wiley- Interscience, US, ISBN: 0-471-51110-2, 1972.

37. Insu Chang, Sang-Young Park, Kyu-Hong Choi, "Decentralized coordinated attitude control for satellite for-mation flying via the state-dependent Riccati equation technique," International Journal of Non-Linear Mechanics 44 (2009) 891 – 904.

38. XU Jin, HU Lifu, "Formation Keeping of Micro-Satellites LQR Control Algorithms Analysis," Proceedings of 2011 International Conference on Electronics and Optoelectronics, Dalian, 29-31 July 2011

39. Fortescue, P., Stark, J. and Swinerd, G. (Eds) Spacecraft Systems Engineering, John Wiley & Sons, Chichester, 2003. ISBN: 0-41-61951-5

40. UNIVERSAL ROBOTS, Parameters for calculations of kinematics and dynamics [online], 26 Feb 2019, Available: https://www.universal-robots.com/how-tos-and-faqs/faq/ur-faq/parameters-for-calculations-of-kinematics-and-dynamics-45257/